Synthesis, Structural Characterization, and Density Functional Study of Homo- and Heteropolyhalide Complexes of Cu^{II} with Dien and Dpta Ligands: Crystal Structure of [Bis(3-aminopropyl)amine](bromo)(diiodobromo)copper(II)

Aikaterini T. Chaviara,[a] Athanasios C. Tsipis,*[b] Philip J. Cox,[c] and Christos A. Bolos*[a]

Keywords: Copper / Density functional calculations / Halides / N ligands

Polyhalide mononuclear $[CuX(L)(XY_2)]$ and dinuclear $[\{CuX(L)\}_2(\mu\text{-}XY_2X)]$ Cu^{II} complexes [L = diethylenetriamine (dien) or dipropylenetriamine (dpta); X = Cl, Br and Y = Br, I] have been obtained by treating the precursor $[CuX_2(L)]$ complexes with Br_2 or I_2 in 1:1 and 2:1 molar ratios. The new homo- and heteropolyhalide Cu^{II} complexes, either mononuclear or dinuclear, were predicted to be five-coordinate Cu^{II} complexes exhibiting a distorted square-pyramidal configuration. DFT calculations at the B3LYP level of theory provided a satisfactory description of the structures of all complexes, while the distorted square-pyramidal structure of a representative complex, namely $[CuBr(dpta)(BrI_2)]$, was further substantiated by a single-crystal X-ray diffraction study. In the square-pyramidal structure of $[CuBr(dpta)(BrI_2)]$, the basal plane of the pyramid involves three Cu–N contacts [1.990(7), 2.065(7), and 1.989(7) Å] from dpta and the Br(1) atom, while Br(2), which participates in the formation of the terminal $[BrI_2]^-$ ligand, occupies the apical position. The Cu–Br(1) and Cu–Br(2) bond lengths were found to be 2.5797(14) Å (terminal) and 2.735(14) Å (bridging), respectively, while the Br1–Cu–Br2 bond angle is 98.83(5)°. The terminal $[BrI_2]^-$ ligand is almost linear [Br–I–I bond angle of 174.48(3)°]. DFT calculations, spectroscopic measurements, including far-IR and EPR studies, and magnetic measurements of the dinuclear complexes predict that the bridging tetrahalide XY_2X moiety adopts a linear configuration as well. The bonding, electronic, and related properties of the complexes are also discussed in the framework of density functional theory.

Introduction

Polyhalides are an interesting class of complex materials, which have drawn the attention of synthetic, theoretical, and applied scientists for many years. The tendency of the heavier halogens, particularly iodine, to form stable polyhalide anions $[X_mY_nZ_p]^-$, (X, Y and Z are identical or different halogen atoms; $m + n + p$ is an odd number that can be 3, 5, 7 or 9) or $[X_4]^{2-}$ dianions of variable stoichiometry has been studied thoroughly.[1–3] The formation of a particular polyhalide species depends not only on the specific halogen (X = I, Br, Cl) but also on the bulkiness and polarizability of the cation, the relative concentrations of the components, and, in some cases, on the synthetic route used.[4] The homo- and heterotrihalide anions $[X_3]^-$ and $[X_2Y]^-$ may be considered as donor–acceptor adducts resulting from the addition of a halide anion (Lewis base) to a halogen or interhalogen molecule (Lewis acids).[5] The bonding in the $[X_3]^-$ species can be described by delocalized three-center four-electron (3c-4e) interactions or, alternatively, by a σ-dative $X \rightarrow X_2$ donor–acceptor interaction.[6] The polyhalide species have found a wealth of applications as useful optical materials,[7] superconducting polymers,[8] electric and magnetic materials,[9] oxidizing[10] or halogenating reagents,[11] recyclable oxidizing reagents,[12] or recyclable reagents for the selective iodination of amines and phenols.[13] The halide ions can be used for the halogenation of organic substrates, thus giving products that are important as potent antitumor, antifungal, antibacterial, antineoplastic, anti-inflammatory, and antiviral agents.[14] Polyhalides are generally prepared[5] by the reaction of an ionic halide with the appropriate halogen under conditions specified by the relevant reactivity of the reactants and products through an ion–dipole interaction. The two reacting species can be combined by direct exposure of the halide to the gaseous halogen, by mixing in an appropriate solvent, by in situ reaction following the production of the interhalogen compound, and finally by the exchange reaction of halogens of different atomic number. The product's stability is governed by the size and the polarizability of the specific halogen atoms.

Although a vast number of polyiodide compounds of univalent cations (Cs^+, K^+, Na^+, NR_4^+) have been pre-

[a] Laboratory of Inorganic Chemistry, Department of General and Inorganic Chemistry, Faculty of Chemistry, Aristotle University of Thessaloniki,
54124 Thessaloniki, Greece
[b] Laboratory of Inorganic Chemistry, Department of Chemistry, University of Ioannina,
451 10 Ioannina, Greece
[c] School of Pharmacy, The Robert Gordon University, Schoolhill,
Aberdeen AB10 1FR, Scotland

pared, the synthetic attempts to synthesize polyhalide coordination compounds of transition metals are limited. In this work we report on the synthesis, structural characterization, electronic structure, and bonding of novel Cu^{II} polyhalide complexes obtained by the reaction of the $[Cu(dien)X_2]$ and $[Cu(dpta)X_2]$ complexes with iodine and bromine. The study of the new halometalate derivatives provides further structural information about different linking motifs of halogen-rich compounds.

Results and Discussion

Synthesis

Mononuclear copper(II) trihalide complexes of the general formula $[CuX(L)(XY_2)]$ and the tetrahalide-bridged dicopper(II) loose associations formulated as $[\{CuX(L)\}_2(\mu\text{-}XY_2X)]$ (L = dien, dpta; X = Cl, Br; Y = Br, I) were prepared by treating the precursor $[CuX_2(L)]$ (L = dien, dpta; X = Cl, Br) complexes with Br_2 or I_2 in 1:1 or 2:1 molar ratios, respectively. The precursor $[CuX_2(L)]$ (X = Br, L = dien, **1**;X = Cl, L = dien, **2**; X = Br, L = dpta, **3**; X = Cl, L = dpta, **4**) complexes undergo ligand dissociation in methanol solution to afford the cation $[CuX(L)]^+$ (L = dien, dpta) and X^- anions. The halide anions formed serve as the nucleophilic active center, thus fulfilling one of the highly desirable criteria of such specific addition reactions. The Cu^{II} polyhalide complexes isolated are deeply colored brown or green, crystalline or amorphous powders that are stable at low temperatures.

Structural Characterization

The new compounds were characterized by elemental analysis (C, H, N, Cu) and spectroscopic (IR, UV/Vis), magnetic, and molar conductivity measurements. Moreover, equilibrium structures of all the complexes studied were determined by electronic structure calculation methods at the B3LYP/LANL2DZ level of theory. Furthermore, the crystal structure of the representative mononuclear complex $[CuBr(dpta)(BrI_2)]$ (**5**) was determined by X-ray crystallography.

Vibrational Spectra

The infrared and far-infrared spectra of the compounds, recorded in the ranges 4000–250 cm^{-1} and 400–100 cm^{-1}, respectively, show all the expected strong bands of the coordinated dien and dpta ligands, which confirms the tridentate[15,16] bonding mode of their coordination to the Cu^{II} centers. The peaks at 255–311 cm^{-1} and 223–311 cm^{-1} are typical of copper halides and are attributed to the ν(Cu–Cl) and ν(Cu–Br) stretching vibrations, respectively, of the terminal halide ligands.[17] The computed unscaled harmonic vibrational frequencies of $[CuX(L)(XY_2)]$ (X = Br, Y = I, L = dien, **5**; X = Cl, Y = Br, L = dpta, **6**; X = Br, Y = Br, L = dien, **7**) and $[\{CuX(L)\}_2(\mu\text{-}XY_2X)]$ (X = Cl, Y = Br, L = dien, **8**; X = Cl, I; L = dpta; **9**, X = Br Y = Br, L = dpta, **10**; X = Br, Y = I, L = dien, **11**), due to ν(Cu–Cl) and ν(Cu–Br) stretching vibrations are found in the regions 220–245 and 170–190 cm^{-1}, respectively. The normal vibrational modes of the polyhalide moieties in **5**–**11** appear in the far-IR region of the spectra as two strong bands located at around 158 and 188 cm^{-1} for the mononuclear complexes and as a weak and very broad band at 123–182 cm^{-1} for the dinuclear ones. The weak, broad band due to the bridging $[X–Y–Y–X]^{2-}$ polyhalide unit, which corresponds to an IR-inactive normal mode, is indicative of the linearity of the tetrahalide bridge; this was further corroborated by the DFT calculations of the equilibrium geometries of the respective compounds. The computed far-infrared harmonic vibrational frequencies due to the stretching and bending vibrational normal modes of the polyhalide moieties, along with their assignments, are compiled in Table 1. Notice that the computed bending modes of the polyhalide moieties in **5**–**11** occur in the same region as $\delta(IBr_2)$ and $\delta(I_3Br)$ of the $[I_3Br_4]^-$ anion in the $[PPh_4][I_3Br_4]$ molecule (72–97 cm^{-1}).[18]

Table 1. Far-infrared harmonic vibrational frequencies [cm^{-1}] due to the vibrational normal modes of the polyhalide moieties of complexes **5–11** computed at the B3LYP/LANL2DZ level.

Complex	Frequency[a]		Assignment
	Calcd.	Exp.	
5	54 (1)		$\delta(BrI_2)$
	116 (8)		ν_s(BrCuBr)
	153 (82)	158 (m)–173 (m)	$\nu_{as}(BrCuBrI_2)$
	163 (5)		$\nu_s(BrCuBrI_2)$
6	77 (1)		$\delta(ClBr_2)$
	174 (35)	170 (m)–188 (m)	$\nu_s(ClBr_2)$
	228 (125)		$\nu_{as}(ClCuClBr_2)$
7	68 (0)		$\delta(Br_3)$
	91 (4)		$\delta(Br_3)$
	119 (15)		$\nu_s(CuBrBr_2)$
	131 (12)	143 (m)–178 (m)	$\nu_s(Br_3)$
	220 (60)		$\nu_{as}(Br_3)$
8	82 (1)		$\delta(ClBr_2)$
	134 (3)	128–181 (w, br)	ν_s(Cl–Br–Br–Cl)
	168 (50)		$\nu_s(ClCuClBr_2)$
	217 (15)		$\nu_{as}(ClCuClBr_2)$
9	58 (1)		$\delta(ClI_2)$
	110 (1)	123 (w, br)	ν_s(Cl–I–I–Cl)
	157 (3)		ν_{as}(Cl–I–I–Cl)
10	23 (0)		δ(Br–Br–Br–Br)
	123 (0)		ν_s(Br–Br–Br–Br)
	140 (2)		ν_s(–Br–Br–)
	188 (5)	160–180 (w, br)	ν_{as}(BrCuBr)
11	61 (6)		$\delta(BrI_2)$
	105 (0)		ν_s(–I–I–)
	122 (97)		ν_{as}(Br–I–I–Br)
	185 (25)	170–180 (w, br)	ν_{as}(BrCuBr)

[a] Figures in parentheses are the intensities of the absorption bands (km mol^{-1}).

Electronic Spectra

The electronic absorption spectra of the complexes in DMF solution and in the solid state (Nujol mulls) exhibit

two or three absorption bands in the ultraviolet and in the visible region of the spectra. To help assignment of the bands and evaluate the properties of the excited states of the Cu^{II} polyhalide complexes, TD-DFT calculations were employed for the precursor complexes **1**–**4** and the mononuclear complexes **5**–**7** in their doublet ground states. Because of the large size of the dinuclear complexes in their triplet ground states, all attempts to compute their principal singlet–singlet electronic transitions were unsuccessful with the computational resources available. The TD-DFT principal singlet–singlet electronic transitions, excitation energies, and oscillator strengths of the mononuclear polyhalide complexes and their precursors are compiled in Table 2.

The computed electronic transitions of the polyhalide Cu^{II} complexes are in excellent agreement with the experimental ones. Thus, all polyhalide complexes exhibit an intense band in the UV region of the spectra at about 360 nm and a broad band in the visible region at 588–645 nm. According to the TD-DFT calculations the high mixing of excited configurations due to the low symmetry of the complexes does not allow us to classify the calculated transitions into the well-known intraligand (LL) or interligand (LL′), ligand-to-metal (LMCT) or metal-to-ligand (MLCT), and ligand field (LF) transitions. The absorption bands arise from electronic transitions between highly delocalized MOs resulting from the mixing of excited configurations having large coefficients in the CI wavefunctions. To intuitively understand the absorption processes, representative density diagrams of the participating MOs for the mononuclear complex **5** are depicted in Figure 1.

For the mononuclear precursor dihalide complexes **1**–**4** the absorption bands in the region of 200–300 nm could be classified as LMCT bands resulting from a combination of dipole-allowed X→Cu and L→Cu (X = Cl, Br; L = dien, dpta) excitations. On the other hand, the absorption bands in the region 300–600 nm correspond to a combination of ligand-field *d*→*d* and X→Cu LMCT transitions. The interligand nature of the LLCT transitions occurring between different ligands of the complexes is worthy of note (Figure 1).

Table 2. Principal electronic transitions, wavelengths (λ), and oscillator strengths (f) for the mononuclear [Cu(L)(X_2)] and [CuX(L)(XY_2)] (L = dien, dpta; X = Cl, Br and Y = Br, I) complexes computed at the B3LYP/LANL2DZ level of theory.

Compound	λ [nm]	f[a]	Assignment
[Cu(dien)Br_2] (**1**)	533	0.0510	LMCT (Br → Cu) + *d* → *d*
	420	0.0768	*d* → *d*
	285	0.0753	LMCT (dien → Cu)
	214	0.0279	LMCT (Br → Cu)
	209	0.0439	LMCT(Br → Cu)
[Cu(dien)Cl_2] (**2**)	565	0.0015	*d* → *d* + LMCT (Cl → Cu)
	448	0.0295	LMCT (Cl → Cu) + *d* → *d*
	369	0.0845	*d* → *d* + LMCT (Cl → Cu)
	278	0.0881	LMCT (dien → Cu)
	202	0.0169	LMCT(Cl → Cu)
[Cu(dpta)Br_2] (**3**)	488	0.0165	LMCT (Br → Cu) + *d* → *d*
	408	0.1184	*d* → *d* + LMCT (Br → Cu)
	334	0.0202	*d* → *d* + LMCT (dpta → Cu)
	276	0.0688	LMCT (dpta → Cu)
	238	0.0305	LMCT (Br → Cu)
	230	0.1092	LMCT (Br → Cu)
	217	0.0429	LMCT (Br → Cu)
[Cu(dpta)Cl_2] (**4**)	457	0.0173	LMCT (Cl → Cu) + *d* → *d*
	373	0.0917	*d* → *d* + LMCT (Cl → Cu)
	320	0.0203	*d* → *d* + LMCT (dpta → Cu
	283	0.1160	LMCT (dpta → Cu)
	196	0.0449	LMCT (dpta → Cu)
[CuBr(dpta)(BrI_2)] (**5**)	754	0.0192	*d* → *d* + LMCT (Br → Cu)
	459	0.0214	LMCT (I_2Br → Cu) + LLCT (I_2Br→ I_2Br)
	404	0.1926	*d* → *d* + LMCT (I_2Br→ Cu)
	324	0.1025	LMCT (I_2Br → Cu) + *d* → *d*
[CuCl(dpta)($ClBr_2$)] (**6**)	737	0.0080	LMCT (Cl → Cu) + *d* → *d*
	352	0.0431	LMCT (Br_2Cl → Cu)
	343	0.0662	LMCT (Cl, Br_2Cl → Cu)
	311	0.0590	*d* → *d* + LMCT (Br_2Cl → Cu)
	278	0.0357	LLCT(dpta→ Br_2Cl)
[CuBr(dien)(Br_3)] (**7**)	757	0.0178	LMCT (Br → Cu) + *d* → *d*
	462	0.0150	LLCT(Br→ Br_3)
	416	0.0174	LMCT (Br_3 → Cu)
	387	0.0197	LLCT(dpta→ Br_3)
	376	0.1215	*d* → *d* + LMCT (Br, Br_3 → Cu)
	330	0.0175	*d* → *d* + LMCT (Br → Cu)
	291	0.1092	MLCT (Cu → Br_3)
	287	0.2934	LMCT (Br → Cu

[a] Only transitions with oscillator strengths larger than 0.015 are considered.

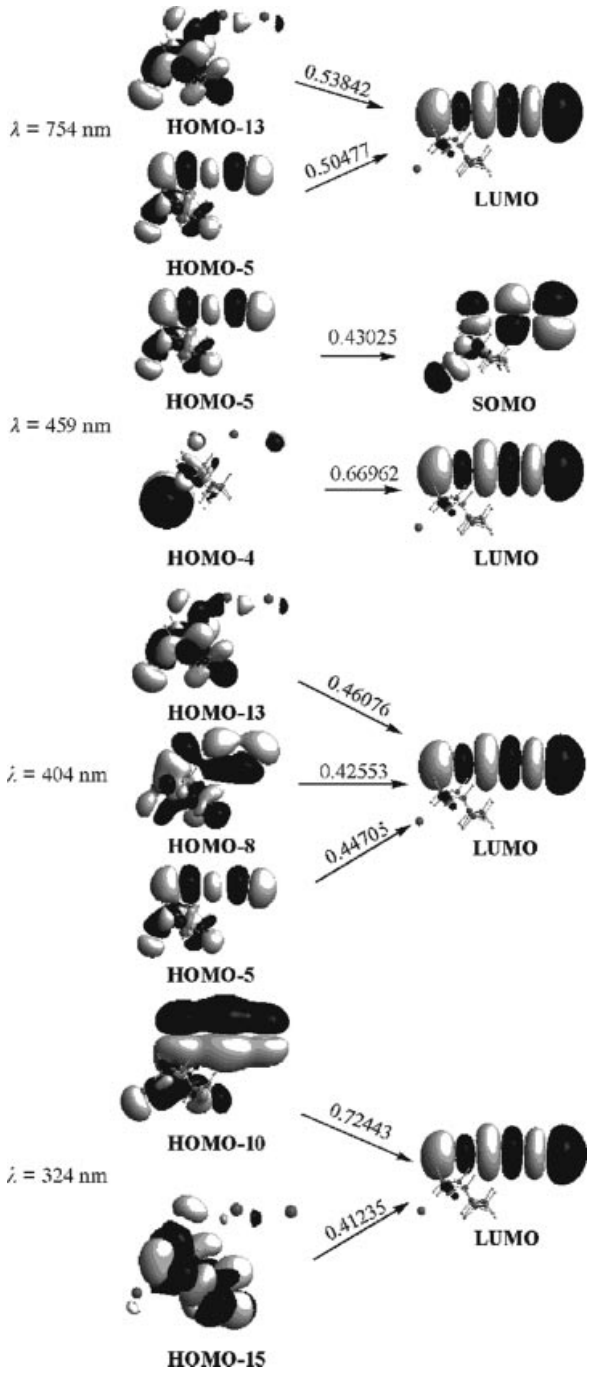

Figure 1. Single-electron transitions with the CI coefficients in the TD-DFT calculations for the more intense bands of [CuBr(dpta)-(BrI_2)] (**5**).

Magnetic Moments, Spin Densities, and Conductivity Measurements

The mononuclear and dinuclear structures of the polyhalide complexes exhibit normal μ_{eff} values per Cu^{II} in the range 1.65–2.19 BM. The room temperature μ_{eff} values of the dinuclear complexes are indicative of a triplet ground state, which was further corroborated by the DFT calculations, as will be discussed later on. In effect, the μ_{eff} values of the complexes are consistent with the computed spin-density distribution. The total spin-density surfaces (SDS) of the polyhalide complexes, along with the numerical values of the spin density at each atom, are displayed in Scheme 1.

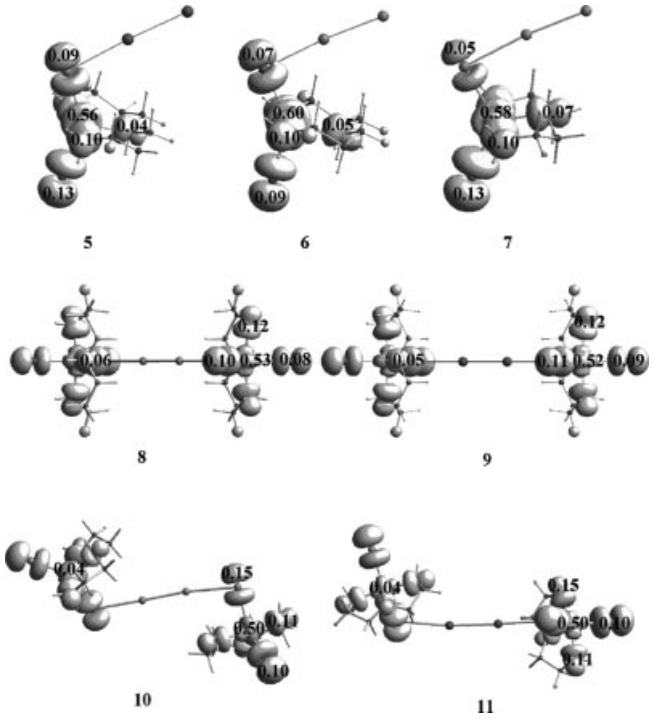

Scheme 1.

It can be seen that the spin density is mainly localized on the central Cu^{II} atoms and the N donor atoms of the dien or dpta ligands. In the dinuclear complexes the spin density distribution follows a similar pattern, but with the spin density localized on the Cu^{II} central atoms being slightly lower, in line with the lower μ_{eff} values of the dinuclear complexes. It is important to note that no spin density is delocalized onto the incoming halogen to form the terminal trihalide or the bridging tetrahalide ligands. Moreover, the computed $<S^2>$ values of 0.754 and 2.005 for the mononuclear and dinuclear complexes, respectively, indicate minimal artificial spin contamination in the calculations.

The molar conductivity measurements of the mononuclear complexes in DMF solution illustrate their essentially 1:1 electrolytic character.[19] As far as the dinuclear complexes are concerned, their $\Lambda\mu$ values are generally slightly higher than those of the mononuclear species, but within the 1:1 range, the only exception being complex **10**, the $\Lambda\mu$ value of which (147 $\mu S\,cm^{-1}$) indicates 2:1 dissociation. The easy dissociation of the dinuclear complexes to mononuclear [$CuX(L)(XY_2)$] ones and the [$CuX_2(L)$] precursors did not allow us, despite many attempts, to isolate crystals suitable for an X-ray diffraction study of their molecular structures. In light of this, the dinuclear complexes can be considered as loose associations between the mononuclear

$[CuX(L)(XY_2)]$ complexes and their $[CuX_2(L)]$ precursors, in line with the DFT results (see below).

Crystal Structure of $[CuBr(dpta)(BrI_2)]$ (5)

A perspective drawing exhibiting the atom numbering is shown in Figure 2.

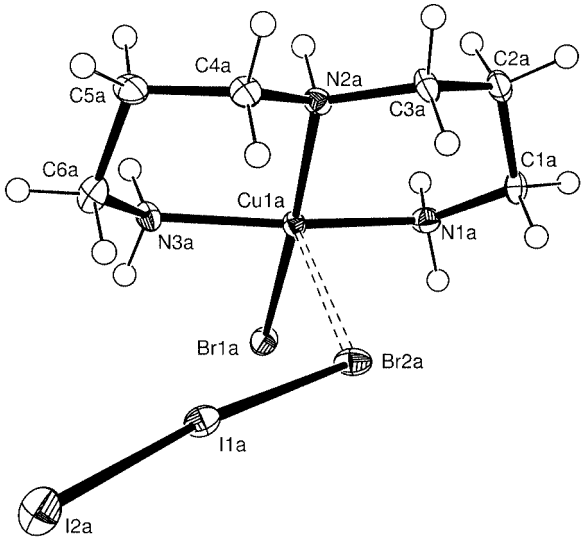

Figure 2. ORTEP plot showing the molecular structure of the $[CuBr(dpta)(BrI_2)]$ with the atom numbering scheme. Thermal ellipsoids are presented at the 50% probability level.

There are 16 formula units per cell and two molecules (**5a** and **5b**) in the asymmetric unit of the structure, with their structural differences being only marginal. Selected bond lengths and angles for **5a** and **5b** are given in Tables 3 and 4, respectively.

Table 3. Selected bond lengths [Å] and angles [°] for **5a**.

I(1A)–I(2A)	2.7619(8)	I(1A)–Br(2A)	2.9484(10)
Br(1A)–Cu(1A)	2.5797(14)	Br(2A)–Cu(1A)	2.7351(14)
Cu(1A)–N(1A)	1.990(7)	Cu(1A)–N(3A)	1.989(7)
Cu(1A)–N(2A)	2.065(7)		
I(2A)–I(1A)–Br(2A)	174.48(3)	Cu(1A)–Br(2A)–I(1A)	119.85(4)
N(1A)–Cu(1A)–N(3A)	162.9(3)	N(3A)–Cu(1A)–N(2A)	92.5(3)
N(1A)–Cu(1A)–N(2A)	94.3(3)	N(3A)–Cu(1A)–Br(1A)	86.6(2)
N(1A)–Cu(1A)–Br(1A)	84.2(2)	N(1A)–Cu(1A)–Br(2A)	92.2(2)
N(2A)–Cu(1A)–Br(1A)	170.4(2)	N(2A)–Cu(1A)–Br(2A)	90.7(2)
N(3A)–Cu(1A)–Br(2A)	103.4(2)	Br(1A)–Cu(1A)-Br(2A)	98.83(5)

The gross geometry of complex **5** appears to be that of a distorted square pyramid and is characterized by *trans*-N–Cu–N (162.9°) and N–Cu–Br (170.4°) bond angles that deviate slightly from the ideal value of 180°. In this distorted CuN_3Br_2 square-pyramidal environment, three nitrogen atoms [N(1A), N(2A) and N(3A)] of the dien or dpta ligands and one bromine atom [Br(1A)] lie in the equatorial plane, whereas the axial position is occupied by the bromine atom [Br(2A)] of the trihalide $[BrI_2]^-$ ligand. The copper atoms Cu(1A) and Cu(1B) are displaced by 0.226(4) and 0.210(4) Å from the plane towards the apical Br(2A) and Br(2B), respectively. The N3–Cu–N2, N2–Cu–N1, N3–Cu–Br1, and Br1–Cu–N1 bond angles in the equatorial plane have values of 92.5(3)°, 94.3(3)°, 86.6(2)°, and 84.2(2)°, respectively, which deviate from the ideal value of 90° for a perfect square plane. The three Cu–N bond lengths span the range of 1.989(7) to 2.065(7) Å, and are consistent with those found in square-pyramidal Cu^{II} complexes with nitrogen donor ligands. The Cu–Br(1) bond length [2.5797(14) Å] in the basal plane is, as expected, shorter than that of the axial Cu–Br(2) bond length [2.7351(14) Å]. Note that the axially coordinated Br(2) atom involved in the formation of the trihalide $[BrI_2]^-$ ligand is not perpendicular to the equatorial plane, the relevant N3–Cu–Br2 and Br1–Cu–Br2 bond angles being 103.4° and 98.83°, respectively. The chair conformation adopted by the six-membered chelate ring formed upon coordination of the dpta ligand to the copper(II) central atom is noteworthy. The trihalide $[BrI_2]^-$ ligand coordinated through the bromine donor atom is almost linear; the Br–I–I bond angle (174.48°) compares well with the respective bond angles of the isostructural CsI_3 (176.3°) and CsI_2Br (178.0°) species. The Br–I bond length of 2.9484 Å is slightly longer than the I–I bond length of 2.7619 Å. These data are in line with the relevant structural features of the $[BrI_2]^-$ moiety in CsI_2Br,[20] which exhibits Br–I and I–I bond lengths of 2.906 and 2.777 Å, respectively.

Table 4. Selected bond lengths [Å] and angles [°] for **5b**.

I(1B)–I(2B)	2.7856(8)	I(1B)–Br(2B)	2.8549(10)
Br(1B)–Cu(1B)	2.5451(13)	Br(2B)–Cu(1B)	2.8118(14)
Cu(1B)–N(1B)	1.991(7)	Cu(1B)–N(3B)	1.984(7)
Cu(1B)–N(2B)	2.060(7)		
I(2B)–I(1B)–Br(2B)	177.50(3)	Cu(1B)–Br(2B)–I(1B)	102.72(4)
N(3B)–Cu(1B)–N(1B)	165.9(3)	N(1B)–Cu(1B)–N(2B)	94.4(3)
N(3B)–Cu(1B)–N(2B)	92.9(3)	N(1B)–Cu(1B)–Br(1B)	83.9(2)
N(3B)–Cu(1B)–Br(1B)	86.6(2)	N(2B)–Cu(1B)–Br(1B)	168.6(2)
N(1B)–Cu(1B)–Br(2B)	95.7(2)	N(3B)–Cu(1B)–Br(2B)	96.2(2)
N(2B)–Cu(1B)–Br(2B)	91.9(2)	Br(1B)–Cu(1B)-Br(2B)	99.50(4)

The equilibrium structures of the whole series of mononuclear and dinuclear polyhalide complexes of Cu^{II} were also determined using computational techniques at the DFT level of theory.

EPR Spectra

The EPR spectrum for powdered $[\{CuBr(dien)\}_2(\mu\text{-}Br_4)]$ and $[\{CuBr(dien)\}_2(\mu\text{-}Br_2I_2)]$ samples (Figure 3) are dominated by a broad derivative centered at $g \approx 2$ plus a weaker feature at $g \approx 4$. Linewidth limitations did not allow us to resolve the hyperfine couplings. The feature at $g \approx 4$ is a semi-forbidden $|\Delta m_s| = 2$ transition[21] that is indicative of pairs of interacting Cu^{II} paramagnetic centers. Similar spec-

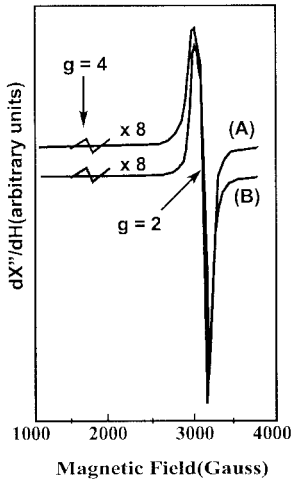

Figure 3. Powder EPR spectrum of powderered [{CuBr(dien)}$_2$(μ-Br_4)] (A) and [{CuBr(dien)}$_2$(μ-Br_2I_2)] (B). Experimental conditions: Temperature: 10.1 K; microwave frequency: 9.42 GHz; modulation amplitude: 10 G peak to peak; microwave power: 32 mW; modulation frequency: 100 kHz. The inset g = 4 signals were recorded using an eightfold larger gain and at 64 mW.

tra have been previously reported for other dinuclear Cu^{II} complexes.[22–24] Accordingly, the present EPR data show that both [{CuBr(dien)}$_2$(μ-Br_4)] and [{CuBr(dien)}$_2$(μ-Br_2I_2)] consist of dinuclear Cu^{II} centers. The details of the lineshape of coupled spin systems depend critically on the relative size of the dipolar and exchange interaction terms, i.e. D and J.[21]

Computational Studies by DFT – Equilibrium Geometry, Electronic Structure, and Bonding Mechanism in Mononuclear Cu^{II} Polyhalide Complexes

The next goal of this work was to determine the details of the electronic structure and, in particular, the nature of the bonding of the polyhalide $[XY_2]^-$ ligand in a series of mononuclear [CuX(L)(XY_2)] (L = dien or dpta; X = Cl, Br and Y = Br, I) compounds and explore the effect of the nature of the halogens on the formation and stability of the polyhalide ligands. Selected geometric, energetic, and electronic parameters for the mononuclear complexes com-

Table 5. Selected structural, energetic, and electronic properties of the mononuclear [CuX(L)(XY_2)] complexes computed at the B3LYP/LANL2DZ level of theory.

	[CuCl(dien)($ClBr_2$)]	[CuCl(dien)(ClI_2)]	[CuBr(dien)($BrBr_2$)]	([CuBr(dpta)($BrBr_2$)])
E [hartrees]	–576.788386	–576.788386	–573.231294	–569.683534
	(–655.351999)	(–655.351999)	(–651.790088)	(–648.246996)
ΔE_1[a] [kcal mol^{-1}]	12.5	12.5	15.8	10.6
	(12.9)	(12.9)	(13.4)	(11.1)
ΔE_2[b] [kcal mol^{-1}]	88.7	88.7	86.2	80.6
	(87.7)	(87.7)	(83.1)	(80.5)
R_e(Cu–X) [Å]	2.339	2.339	2.566	2.531
	(2.480)	(2.480)	(2.669)	(2.658)
R_e(Cu–XY_2) [Å]	2.603	2.603	2.693	2.709
	(2.514)	(2.514)	(2.740)	(2.691)
R_e(X–Y) [Å]	2.760	2.760	2.898	3.129
	(2.775)	(2.775)	(2.901)	(3.120)
R_e(Y–Y) [Å]	2.630	2.630	2.658	2.976
	(2.624)	(2.624)	(2.648)	(2.976)
X–Cu–X [°]	131.2	131.2	131.5	133.6
	(137.7)	(137.7)	(135.2)	(143.8)
Cu–X–Y [°]	103.0	103.0	90.5	107.2
	(90.8)	(90.8)	(84.4)	(100.0)
X–Y–Y [°]	175.1	175.1	174.1	176.4
	(174.8)	(174.8)	(173.8)	(176.8)
μ_e [D]	10.3	10.3	6.5	7.8
	(5.1)	(5.1)	(4.9)	(5.6)
η [eV]	1.62	1.62	1.46	1.41
	(1.50)	(1.50)	(1.42)	(1.41)
Q(Cu)	0.28	0.28	0.23	0.22
	(0.25)	(0.25)	(0.23)	(0.22)
Q(XY_2)	–0.38	–0.38	–0.27	–0.35
	(–0.34)	(–0.34)	(–0.45)	(–0.34)
Q(Y_{int})	–0.05	–0.05	–0.09	–0.06
	(–0.05)	(–0.05)	(–0.08)	(–0.06)
Q(Y_{term})	–0.22	–0.22	–0.24	–0.20
	(–0.22)	(–0.22)	(–0.23)	(–0.21)
bop(X–Y_{int})	0.013	0.013	0.016	0.008
	(0.010)	(0.010)	(0.010)	(0.005)

[a] $\Delta E_1 = \{[E_{[CuX_2(L)]} + E_{(Y_2)}] - E_{[CuX(L)(XY_2)]}\}$. [b] $\Delta E_2 = \{[E_{[CuX(L)]^+} + E_{(XY_2)^-}] - E_{[CuX(L)(XY_2)]}\}$.

puted at the B3LYP/LANL2DZ level of theory are compiled in Table 5.

It can be seen that the B3LYP/LANL2DZ calculations reproduce well the molecular structure of complex **5** determined by X-ray crystallography. In all mononuclear complexes the trihalide $[XY_2]^-$ ligand adopts an almost linear configuration with the X–Y–Y bond angle ranging from 173.8° up to 176.8°. The $[XY_2]^-$ ligand occupying the axial position in the distorted square pyramidal geometry of the complexes is coordinated to the Cu^{II} central atom in a bent fashion. The computed Cu–X–Y bond angles found in the range of 84.4–107.2° depend on the nature of the halides involved in the formation of the $[XY_2]^-$ ligands. In general terms, the Cu–X–Y bond angles are smaller in the dpta than in the dien complexes.

The association of the incoming Y_2 molecule with the halide X^- ligand to afford the coordinated trihalide $[XY_2]^-$ ligand corresponds to a relatively weak interaction. The association energies, ΔE_1, computed at the B3LYP/LANL2DZ level of theory amount to only 10.6–15.8 kcal mol^{-1} and are comparable to those of hydrogen bonds. However, the trihalide $[XY_2]^-$ ligands interact strongly with the Cu^{II} central atom, the computed Cu–XY_2 bond-dissociation energy, ΔE_2, being 80.5–88.7 kcal mol^{-1}.

Generally, the trihalide $[XY_2]^-$ ligands form slightly stronger coordination bonds in the dien than in the dpta complexes. In both series of complexes the ΔE_2 values follow the trend $[ClBr_2]^- > [ClI_2]^- > [Br_3]^- > [BrI_2]^-$.

Upon association of the Y_2 molecule with the halide X^- ligand there is a charge transfer from the X^- ligand towards the Y_2 molecule, with the transferred electron density mainly localized on the terminal Y atom, which acquires a negative net atomic charge of about –0.20 to –0.24 charge units. The internal Y atom acquires only –0.02 to –0.09 charge units. Moreover, the X atom of the coordinated $[XY_2]^-$ ligands acquires a negative net atomic charge amounting to about –0.27 to –0.45 charge units. Obviously, repulsive electrostatic interactions of the negatively charged X and Y_{int} atoms in the $[XY_2]^-$ ligands do exist, therefore the weak X···Y_{int} interactions could be attributed to covalent interactions. In effect, the X···Y_{int} bonding mechanism could be described as donor–acceptor interactions with the incoming Y–Y molecule acting as acceptor through its σ* LUMO, and the coordinated halide ligand X of the $[CuX(L)(XY_2)]$ mononuclear complex acting as the donor through the HOMO, which is mainly localized on that ligand (Scheme 2). These donor–acceptor interactions give rise to both charge transfer from the donor to the acceptor and weakening of the bonding within the acceptor through partial accumulation of electron density on the antibonding σ* LUMO of the acceptor, which is reflected in the elongation of the Y–Y bond length by 0.099 to 0.148 Å. A thorough search of the molecular orbitals of the trihalide complexes reveals that there are bonding MOs describing the X···Y_{int} interactions. Such MOs, along with the doubly degenerate singly occupied (SOMO) and the lowest unoccupied (LUMO) MOs for a representative complex **5** and its precursor complex **1** are also displayed in Scheme 2.

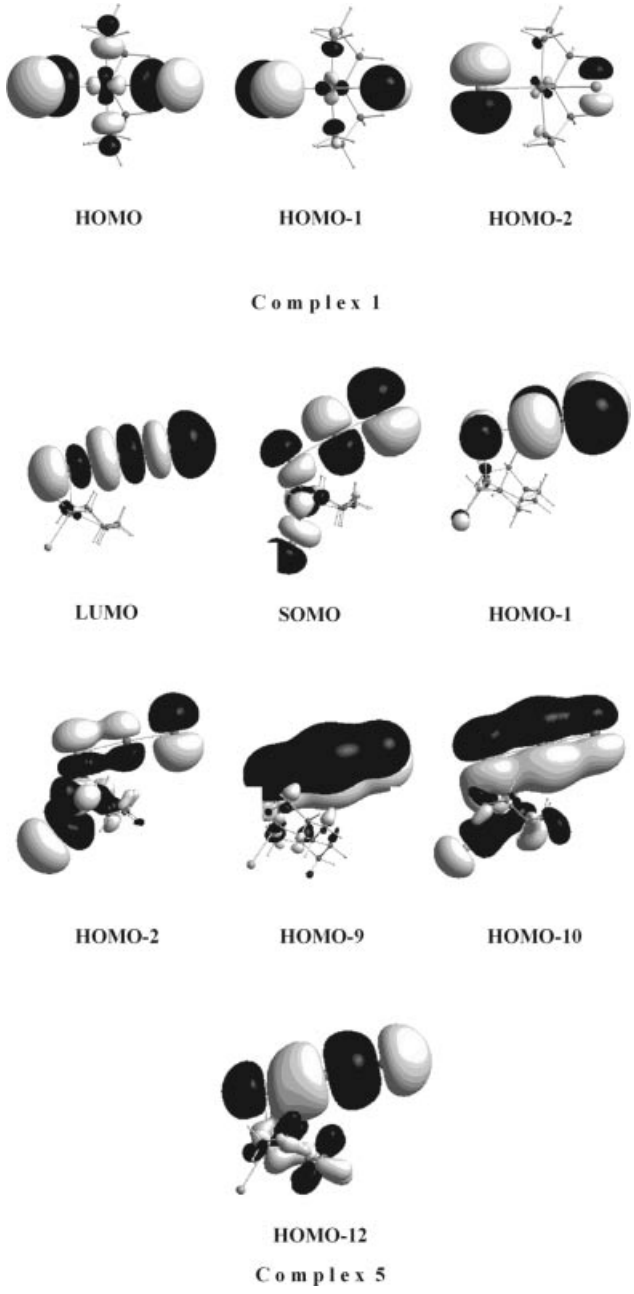

Scheme 2.

The multicenter bonding interactions in HOMO-9 and HOMO-10 and the antibonding ones in SOMO and HOMO-1 should be noted. The HOMO-9 and HOMO-10 correspond to π MOs constructed from the p_π orbitals of the halogen atoms of the X–Y–Y moiety, while the HOMO-12 is a σ-type MO constructed from the p_σ orbitals of the halogen atoms of the X–Y–Y moiety. The SOMO and HOMO-1 correspond to the antibonding π* counterparts of the π_{XYY} MOs. On the other hand, the LUMO corresponds to a σ* MO resulting from the antibonding interaction of p_σ orbitals of the halogen atoms of the X–Y–Y moiety. The computed bond overlap population (bop) values of the X···Y_{int} bonds (Table 5) illustrate the weak nature of the X···Y_{int} interactions. In general terms, these interactions

follow the trend $Br\cdots Br_{int} > Cl\cdots Br_{int} > Br\cdots I_{int} > Cl\cdots I_{int}$, thus suggesting that the strength of the $X\cdots Y_{int}$ interactions increases as the difference of electronegativity of the constituent halogen atoms decreases. Finally, the hardness, η, given by $(\varepsilon_{LUMO} - \varepsilon_{HOMO})/2$, was found to be in the range of 1.41–1.62 eV; it reflects the relative stability of the complexes (Table 5).

Equilibrium Geometry, Electronic Structure, and Bonding Mechanism in Dinuclear Cu^{II} Polyhalide-Bridged Complexes

The dinuclear [{CuX(L)}$_2$(μ-XY$_2$X)] (L = dien, dpta; X = Cl, Br and Y = Br, I) complexes adopt the triplet ground state. The singlet states correspond to local minima in the PES and are 33–37 kcal mol^{-1} higher in energy than the triplet ground states. Selected geometric, energetic, and electronic parameters for the dinuclear complexes computed at the B3LYP/LANL2DZ level of theory are compiled in Table 6.

The two metal centers in the dinuclear complexes exhibit the same stereochemistry, being five coordinate with a distorted square-pyramidal geometry resembling that of the respective precursor [CuX$_2$(L)] complexes. This is indicative of the loose association of the Y$_2$ molecule with the two [CuX$_2$(L)] moieties. The computed dissociation energy of the Y$_2$ molecule from the dinuclear complexes amounts to 15.1–18.3 kcal mol^{-1} at the B3LYP/LANL2DZ level. On the other hand, the dissociation energy of the dinuclear complexes to the [CuX$_2$(L)] and [CuX(L)(XY$_2$)] species was predicted to be only 2.5–4.6 kcal mol^{-1}, thus illustrating that the dinuclear complexes are easily dissociated into the more stable mononuclear [CuX(L)(XY$_2$)] species. The weak X···Y interaction is mirrored by the relatively long X···Y distances (Table 6).

The trihalide [XY$_2$] moiety in all dinuclear complexes is almost linear, with the X–Y–Y bond angle ranging from 174.3° up to 176.8°. However, the Cl–Br–Br–Cl (complex **8**) and Cl–I–I–Cl (complex **9**) bridging units are almost linear, with the torsion angles being about 177°, while the Br–Br–Br–Br (complex **10**) and Br–I–I–Br (complex **11**) bridging units form dihedral angles of 144.9 and –86.5°, respectively. These configuration preferences of the X–Y–Y–X bridging units could be due to electronegativity effects.

The bonding mechanism of the Y$_2$ molecule from each side with the halide X$^-$ ligands of the two mononuclear [CuX$_2$(L)] species corresponds to donor–acceptor interactions giving rise to both a charge transfer from the X$^-$ donor ligands to Y acceptor atoms while the orbital interactions result in the weakening of the Y–Y bond. Both Y atoms acquire a negative net atomic charge of about –0.15 charge units. On the other hand, the elongation of the Y–Y bond length by 0.123 to 0.165 Å is, as expected, higher in the dinuclear than in the mononuclear complexes. A search of the molecular orbitals of the dinuclear complexes reveals that the presence of bonding MOs that describe the X···Y···Y···X interactions. The relevant MOs, along with the doubly degenerate SOMOs and the LUMO for a representative complex (**9**), are displayed in Scheme 3.

Conclusions

In this paper we have reported the synthesis, structural characterization, and DFT study of novel mono- and dinuclear polyhalide Cu^{II} complexes with general formulae [CuX(L)(XY$_2$)] and [{CuX(L)}$_2$(μ-XY$_2$X)] (L = dien or dpta; X = Cl, Br and Y = Br, I). The vibrational spectra confirm the tridentate bonding mode of the dien or dpta ligands to the central Cu^{II} atom and show the characteristic bands related to polyhalide moieties, thus indicating the lin-

Table 6. Selected structural, energetic, and electronic properties of the dinuclear [{CuX$_2$(L)}$_2$(μ-XY$_2$X)}] (L = dien, dpta; X = Cl, Br and Y = Br, I) complexes computed at the B3LYP/LANL2DZ level of theory.

Property	**8**	**9**	**10**	**11**
E_T [hartrees]	–1284.382307	–1280.839568	–1120.133222	–1116.588499
E_S [hartrees]	–1284.324165	–1280.780849	–1120.076554	–1116.535873
ΔE_{T-S}[a] [kcal mol^{-1}]	–36.5	–36.8	–35.4	–33.0
ΔE_1[b] [kcal mol^{-1}]	4.6	4.2	2.5	4.5
ΔE_2[c] [kcal mol^{-1}]	17.5	15.4	18.3	15.1
R_e(Cu–X) [Å]	2.538	2.525	2.545	2.539
R_e(Cu–XY$_2$) [Å]	2.463	2.447	2.673	2.675
R_e(X–Y) [Å]	2.974	3.165	3.135	3.307
R_e(Y–Y) [Å]	2.654	2.986	2.675	3.002
X–Cu–X [°]	135.6	139.6	141.6	138.2
Cu–X–Y [°]	85.0	95.0	100.8	110.4
X–Y–Y [°]	175.6	176.6	174.3	176.8
X–Y–Y–X [°]	176.7	–177.4	144.9	–86.5
μ_e [D]	0.11	0.26	5.8	7.1
η [eV]	1.39	1.50	1.36	1.41
Q(Cu)	0.23	0.23	0.20	0.20
Q(X)	–0.50	–0.49	–0.41	–0.40
Q(**X**Y$_2$)	–0.37	–0.39	–0.37	–0.39
Q(Y)	–0.15	–0.14	–0.18	–0.15

[a] $\Delta E_{T-S} = E_T - E_S$. [b] $\Delta E = [E_{[CuX_2(L)]} + E_{[CuX(L)(XY_2)]} - E_{[\{CuX(L)\}_2(\mu\text{-}XY_2X)\}]}$. [c] $\Delta E = [2E_{[CuX(L)]^+} + E_{Y_2}] - E_{[\{CuX_2(L)\}_2(\mu\text{-}XY_2X)\}]}$.

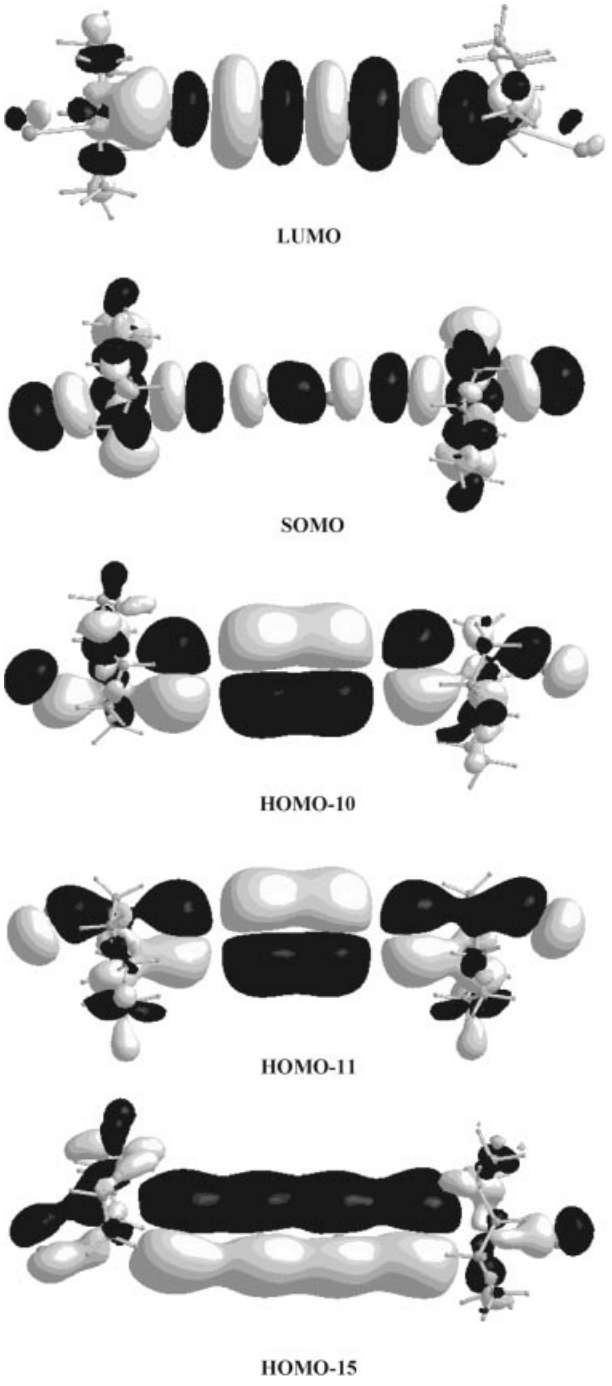

Scheme 3.

earity of the $[X–Y–Y–X]^{2–}$ tetrahalide bridges. According to X-ray data the mononuclear $[CuBr(dpta)(BrI_2)]$ complex adopts a distorted square-pyramidal structure with the apical position occupied by a Br atom that participates in the linear terminal $[BrI_2]^–$ ligand. On the other hand, DFT calculations support a distorted square-pyramidal structure for the $[CuX(L)(XY_2)]$ complexes, in agreement with the experimental findings. The Y_2 molecule in these complexes is weakly bound to the $X^–$ anion, with association energies estimated to be 10.6–15.8 kcal mol$^{–1}$ at the B3LYP/LANL2DZ level. In contrast, the Cu–XY_2 bond-dissociation energies are much larger (80.5–88.7 kcal mol$^{–1}$). The Cu–XY_2 BDEs, which are higher in the dpta than the dien complexes, follow the trend $[ClBr_2]^– > [ClI_2]^– > [Br_3]^– > [BrI_2]^–$.

Both X and Y_{int} atoms in the $[XY_2]^–$ ligand acquire negative charges that give rise to a weak electrostatic interaction. The quite long X···Y_{int} separation distance could be ascribed as a donor–acceptor interaction, with the incoming Y_2 molecule acting as the acceptor through its σ* LUMO and the coordinated $X^–$ ligand being the donor through the HOMO of the $[CuX(L)(XY_2)]$ complex, which is mainly localized on the halide ligands.

The dinuclear $[\{CuX(L)\}_2(\mu\text{-}XY_2X)]$ complexes adopt a triplet ground state while the singlet state corresponds to a local minimum that is about 33–37 kcal mol$^{–1}$ higher in energy. This is corroborated by the μ_{eff} values of the dinuclear complexes, which point to a triplet ground state without any appreciable magnetic interaction. The two metal centers exhibit a distorted square-pyramidal geometry resembling that of the mononuclear $[CuX(L)(XY_2)]$ complexes. The dinuclear $[\{CuX(L)\}_2(\mu\text{-}XY_2X)]$ complexes can easily dissociate into $[CuX(L)(XY_2)]$ and $[CuX_2(L)]$ species due to the very weak X–Y_2 interactions (BDEs are only 2.5–4.6 kcal mol$^{–1}$). The $[XY_2]$ moiety in all dinuclear complexes is almost linear. Finally, the bonding mechanism in the dinuclear $[\{CuX(L)\}_2(\mu\text{-}XY_2X)]$ complexes is described by donor–acceptor interactions which give rise to both charge transfer from the coordinated $X^–$ ligands to the Y_2 moiety at each side and orbital interactions resulting in the elongation of the Y–Y bond, which is greater in the dinuclear than in mononuclear complexes.

Experimental Section

Materials and Instruments: All chemicals were purchased from Aldrich, EDH Chemicals, or Merck and were reagent grade. Carbon, hydrogen, and nitrogen were determined by microanalysis using a Perkin–Elmer 2400 elemental analyser. Copper was determined with a Perkin–Elmer model 403 Atomic Absorption Spectrometer equipped with the appropriate hollow cathode lamps. Molar conductivities were measured with a WTW conductivity bridge employing a calibrated dip-type cell and $10^{–3}$ M solutions in DMF. Magnetic susceptibility measurements on powder samples were performed at room temperature (25 °C) employing the Faraday method with a home-built balance calibrated against $Hg[Co(NCS)_4]$. Diamagnetic corrections were estimated from Pascal's constants. Infrared spectra were obtained by the KBr disc technique and were recorded with a Perkin–Elmer FT-IR Spectrum One spectrometer. Far-infrared spectra (400–100 cm$^{–1}$) were recorded for polyethylene disks with a Bruker 113V Spectrum spectrometer. A 6.25-μm thickness Mylar beam splitter was used for these studies. Electronic spectra in DMF solutions (range 200–1100 nm) and in solid state (Nujol mull, range 400–1100 nm) were measured with a Shimadzu 160A instrument in the range 200–1100 nm. Continuous-wave EPR spectra were recorded at liquid helium temperatures with a Bruker ER 200D X-band spectrometer equipped with an Oxford Instruments cryostat. The microwave frequency and the magnetic field were measured with a microwave frequency counter HP 5350B and a Bruker ER035 M NMR-gaussmeter, respectively.

Computational Details: The structural, electronic, and energetic properties of all compounds were computed with the Becke three-parameter hybrid functional[25,26] combined with the Lee–Yang–Parr correlation functional,[27] abbreviated as B3LYP, using the LANL2DZ basis set[28] that includes Dunning–Huzinaga full double-ζ on the first row and Los Alamos ECPs plus DZ on the copper and halogen atoms. This hybrid B3LYP functional was used since it gives acceptable results for molecular energies and geometries, as well as proton donation, and weak and strong H-bonds.[29–35] No constraints were imposed on the geometry in any of the computations. Full geometry optimization was performed for each structure using Schlegel's analytical gradient method,[36] and the attainment of the energy minimum was verified by calculating the vibrational energy that results in the absence of imaginary eigenvalues. All the stationary points were identified for minimum (number of imaginary frequencies NIMAG = 0) or transition states (NIMAG = 1). Time-dependent density functional theory (TD-DFT)[37–39] calculations were performed on the equilibrium ground state geometries employing the same density functionals and basis sets as used in the geometry optimization. The Davidson algorithm was used, in which the error tolerance in the square of the excitation energies and trial-vector orthonormality criterion were set to 10^{-8} and 10^{-10}, respectively. The success of the TD-DFT method in calculating excitation energies of transition metal complexes has been demonstrated in several recent studies.[40–42] All calculations were performed using the GAUSSIAN03 series of programs.[43] The qualitative concepts and the graphs derived from the Chem3D program suite[44] highlight the basic interactions resulting from the DFT calculations.

Synthesis of the Complexes: The precursors [$CuBr_2$(dien)] (**1**) and [$CuCl_2$(dien)] (**2**) were prepared by literature methods,[45] while the analogous complexes [$CuBr_2$(dpta)] (**3**) and [$CuCl_2$(dpta)] (**4**) were prepared as described below.

[$CuBr_2$(dpta)] (3): dpta (1.41 mL) was added dropwise to a methanolic suspension (ca. 30 mL) containing 2.23 g (10^{-2} mol) of $CuBr_2$. After vigorous stirring for 20 min, a blue precipitate was formed, which was then separated by filtration, washed several times with diethyl ether, and dried in vacuo. Yield: 2.16 g (61%).

[$CuCl_2$(dpta)] (4): The [$CuCl_2$(dpta)] complex, due to its high solubility in methanol, cannot be isolated, therefore the trihalide [CuCl(dpta)($ClBr_2$)] and the tetrahalide [{Cu(dpta)Cl}$_2$(μ-Cl_2I_2)] complexes were prepared in situ.

[CuBr(dpta)(BrI_2)] (5): A methanolic solution (20 mL) of I_2 (1.27 g, 5 mmol) was added dropwise to a methanolic suspension (30 mL) of [$CuBr_2$(dpta)] (1.775 g, 5 mmol). Diethyl ether (10 mL) was added to the resulting dark-green solution, which was further left at low temperature (4 °C) for 24 h, after which the formation of high-quality, dark-green crystals suitable for X-ray diffraction analysis was observed. The crystals formed were isolated by filtration and dried in air. Yield: 1.61 g (53%). $C_6H_{17}Br_2CuI_2N_3$ (608.38): calcd. C 11.84, H 2.82, Cu 10.44, N 6.91; found C 12.00, H 2.83, Cu 10.25, N 6.96. IR: ṽ = 3277 s, 3203 ws, 3126 vs, 504 m, 252 w, 223 cm^{-1} w. Λ_μ (DMF) = 68 μS cm^{-1}. UV/Vis (DMF): λ_{max} (log ε) = 680 nm (2.42); (Nujol): λ_{max} = 740, 451, 410 nm. μ_{eff} = 1.85 μ_B.

[CuCl(dpta)($ClBr_2$)] (6): A methanolic solution containing 1.41 mL of dpta was added to a solution of $CuCl_2 \cdot 2H_2O$ (1.71 g, 10 mmol) in the same solvent. Br_2 (0.55 mL in 10 mL of methanol) was added to the resulting blue solution. After 1 h, the solution was filtered to remove any impurities, ethanol (10 mL) was added to the filtrate, and the brown precipitate was isolated by filtration, washed several times with ethanol and diethyl ether, and dried in vacuo to give red brown microcrystals of **6** (1.19 g, 28%). $C_6H_{17}Br_2Cl_2CuN_3$ (425.38): calcd. C 16.94, H 4.03, Cu 14.93, N 9.88; found C 17.10, H 4.11, Cu 14.80, N 9.85. IR: ṽ = 3260 vs, 3205 vs, 3113 vs, 511 w, 383 w, 326 cm^{-1} w. Λ_μ (DMF) = 75 μS cm^{-1}. UV/Vis (DMF): λ_{max} (log ε) = 720 (1.97), 921 sh, 434 nm sh; (Nujol): λ_{max} = 792, 530 sh, 461 nm sh. μ_{eff} = 1.65 μ_B.

[CuBr(dien)(Br_3)] (7): A methanolic solution (ca. 5 mL) of 0.1 mL of Br_2 was added to another methanolic solution (ca. 20 mL) of [$CuBr_2$(dien)] (0.650 g, 2 mmol). Upon addition, the blue solid turned green. After stirring for 30 min, the solid formed was separated by filtration, washed several times with diethyl ether, and dried in vacuo to give green microcrystals of **7** (0.272 g, 28%). $C_4H_{13}Br_4CuN_3$ (486.33): calcd. C 9.88, H 2.68, Cu 13.06, N 8.64; found C 9.78, H 2.56, Cu 13.20, N 8.57. IR: ṽ = 3290 vs, 3230 vs, 3157 vs, 523 w, 336 w, 315 cm^{-1} w. Λ_μ (DMF) = 82 μS cm^{-1}. UV/Vis (DMF): λ_{max} (log ε) = 618 nm (2.21); (Nujol): λ_{max} = 651, 444, 403 nm sh. μ_{eff} = 2.19 μ_B.

[{CuCl(dien)}$_2$(μ-Cl_2Br_2)] (8): [$CuCl_2$(dien)] (4.75 g, 20 mmol) was dissolved in ca. 30 mL of methanol. After 30 min of vigorous stirring, 0.55 mL of Br_2 in 10 mL of methanol was added and the color of the solution turned from blue to green. The green solid formed was then separated by filtration, washed several times with diethyl ether, and dried in vacuo to give green microcrystals of **8** (4.51 g, 71%). $C_8H_{26}Br_2Cl_4Cu_2N_6$ (635.04): calcd. C 15.13, H 4.13, Cu 20.01, N 13.23; found C 15.23, H 4.20, Cu 19.85, N 13.36. IR: ṽ = 3300 vs, 3244 vs, 3169 vs, 516 w, 383 w, 311 cm^{-1} w. Λ_μ (DMF) = 106 μS cm^{-1}. UV/Vis (DMF): λ_{max} (log ε) = 683 (2.01), 902 nm (1.92); (Nujol): λ_{max} = 684, 449, 404 nm sh. μ_{eff} = 1.89 μ_B.

[{CuCl(dpta)}$_2$(μ-Cl_2I_2)] (9): A methanolic solution of 1.41 mL of dpta was added to a solution of $CuCl_2 \cdot 2H_2O$ (1.71 g, 10 mmol) in 20 mL of methanol. A solution of iodine (1.27 g, 5 mmol) in 20 mL of methanol was added to the resulting blue solution. After 1 h of stirring, the green solution was left to stand and then 10 mL of diethyl ether was added. After 1 h, a microcrystalline dark-green product had formed, which was isolated by filtration, washed twice with 5 mL of diethyl ether and dried in vacuo to give green microcrystals of **9** (2.24 g, 57%). $C_{12}H_{34}Cl_4Cu_2I_2N_6$ (785.15): calcd. C 18.36, H 4.36, Cu 16.19, N 10.70; found C 18.69, H 4.40, Cu 16.01, N 10.56. IR: ṽ = 3250 vs, 3207 vs, 3130 vs, 506 m, 338 w, 255 cm^{-1} w. Λ_μ (DMF) = 88 μS cm^{-1}. UV/Vis (DMF): λ_{max} (log ε) = 647 nm sh; (Nujol): λ_{max} = 783, 460 nm sh. μ_{eff} = 1.76 μ_B.

[{CuBr(dien)}$_2$(μ-Br_4)] (10): A methanolic solution (ca. 5 mL) of 0.15 mL of Br_2 was added to another methanolic solution (ca. 20 mL) of [$CuBr_2$(dien)] (1.63 g, 5 mmol). Upon addition, the blue solid turned dark blue. After stirring for 30 min, the solid formed was separated by filtration, washed several times with diethyl ether, and dried in vacuo to give dark-green microcrystals of **10** (1.04 g, 51%). $C_8H_{26}Br_6Cu_2N_6$ (812.85): calcd. C 11.82, H 3.22, Cu 15.63, N 10.34; found C 11.76, H 3.32, Cu 15.49, N 10.29. IR: ṽ = 3300 vs, 3235 vs, 3125 vs, 518 w, 253 w, 246 cm^{-1} w. Λ_μ (DMF) = 142 μS cm^{-1}. UV/Vis (DMF): λ_{max} (log ε) = 598 (2.55), 941 nm (2.12); (Nujol): λ_{max} = 633 sh, 526, 425 nm sh. μ_{eff} = 2.16 μ_B.

[{CuBr(dien)}$_2$(μ-Br_2I_2)] (11): A methanolic solution (ca. 20 mL) of I_2 (0.254 g, 1 mmol) was added to another methanolic solution (20 mL) of [$CuBr_2$(dien)] (0.65 g, 2 mmol). Upon addition, the blue solid turned brown. After stirring for 30 min, the solid formed was separated by filtration, washed several times with diethyl ether, and dried in vacuo to give black microcrystals of **11** (0.79 g, 88%). $C_8H_{26}Br_4Cu_2I_2N_6$ (906.85): calcd. C 10.60, H 2.89, Cu 14.01, N 9.27; found C 10.686, H 2.97, Cu 14.10, N 9.33. IR: ṽ = 3286 s, 3233 vs, 3161 vs, 516 w, 238 cm^{-1} w. Λ_μ (DMF) = 110 μS cm^{-1}. UV/

Vis (DMF): λ_{max} (log ε) = 617 nm (2.46); (Nujol): λ_{max} = 742, 572, 463, 399 nm. μ_{eff} = 1.99 μ_B.

X-ray Crystallographic Study: X-ray diffraction data were collected with an Enraf–Nonius Kappa CCD area-detector diffractometer. The programs DENZO[46] and COLLECT[47] were used in data collection and cell refinement. Details of data collection and structure refinement are given in Table 7. All crystals produced were twinned such that the data set obtained for a single crystal contained overlapping reflections. After removal of the affected reflections, 51.9% of the data set remained. The structure was solved with the program SIR97[48] and refined with SHELX-97.[49] Molecular plots were obtained with the program ORTEP-3.[50] CCDC-260389 contains the supplementary crystallographic data for this paper. These data can be obtained free of charge from The Cambridge Crystallographic Data Centre via www.ccdc.cam.ac.uk/data_request/cif.

Table 7. Crystal data and structure refinements for [CuBr(dpta)-(BrI_2)] (**5**).

Empirical formula	$C_6H_{17}Br_2CuI_2N_3$
Formula mass	608.39
Temperature	120(2) K
Wavelength	0.71073 Å
Crystal system	monoclinic
Space group	*C*2/*c*
Unit cell dimensions	a = 26.7159(13) Å, α = 90°
	b = 9.01969(10) Å, β = 96.097(3)°
	c = 25.4078(7) Å, γ = 90°
Volume	6087.9(3) $Å^3$
Z	16
Density (calculated)	2.655 $Mg\,m^{-3}$
Absorption coefficient	10.717 mm^{-1}
F(000)	4464
Crystal size	0.32 × 0.18 × 0.08 mm
θ range for data collection	5.04–27.50°
Index ranges	$-34 \le h \le 34$
	$-11 \le k \le 11$
	$-31 \le l \le 31$
Reflections collected	15827
Independent reflections	3633 [R(int) = 0.0403]
Refinement method	Full-matrix least squares on F^2
Data/restraints/parameters	3633/0/254
Goodness-of-fit on F^2	1.082
Final R indices [$I > 2\sigma(I)$]	R_1 = 0.0350, wR_2 = 0.0802
R indices (all data)	R_1 = 0.0521, wR_2 = 0.0846
Largest difference peak/hole	0.838/–0.955 e $Å^{-3}$

Acknowledgments

The financial support of this work by the Greek General Secretariat for Research and Technology and the European Commission within the framework of the PENED01 projects is gratefully acknowledged (grant no. 01EΔ367). We would like to thank Assistant Professor J. Deligiannakis for providing the EPR data and also the EPSRC X-ray crystallography service at the University of Southampton for collecting the X-ray data.

[1] E. Dubler, L. Linowsky, *Helv. Chim. Acta* **1975**, *58*, 2604.
[2] A. Rabenau, H. Schulz, W. Stoeger, *Naturwissenschaften* **1976**, *63*, 245.
[3] M. F. Belicchi, G. G. Fava, C. Pelizzi, *Acta Crystallogr., Sect. B* **1981**, *37*, 924.
[4] E. M. Nour, L. H. Chen, J. Laane, *J. Phys. Chem.* **1986**, *90*, 2841.
[5] J. C. Bailar, H. J. Emeleus, R. Nyholm, A. F. Trotman-Dickenson, *Comprehensive Inorganic Chemistry*, Pergamon Press, Oxford, **1973**, vol. 2.
[6] P. Deplano, J. R. Ferraro, M. L. Mercuri, E. F. Trogu, *Coord. Chem. Rev.* **1999**, *188*, 71.
[7] A. Tracz, J. K. Jeszka, J. Ulanski, T. Pakula, J. P. Rabe, *Synth. Met.* **1998**, *94*, 17.
[8] J. Ulanski, A. Tracz, J. K. Jeszka, E. Laukhina, T. Pakula, *Synth. Met.* **1997**, *85*, 1591.
[9] H. Mittag, P. Cikmacs, H. Fullbier, A. Lusis, G. Petrovskis, L. Schmidt, H. Stegemann, *Soviet Electrochem.* **1989**, *25*, 717.
[10] T. Okamoto, T. Utsunomiya, T. Uesugi, T. Kakinami, S. Kajigaeshi, *Bull. Chem. Soc. Jpn.* **1989**, *62*, 3748.
[11] T. Kakinami, H. Suenaga, T. Yamaguchi, T. Okamoto, S. Kajigaeshi, *Bull. Chem. Soc. Jpn.* **1989**, *62*, 3373.
[12] S. S. Mitra, K. Sreekumar, *Eur. Polym. J.* **1998**, *34*, 561.
[13] S. S. Mitra, K. Sreekumar, *React. Funct. Polym.* **1997**, *32*, 281.
[14] A. Butler, J. V. Walker, *Chem. Rev.* **1993**, *93*, 1937.
[15] K. Nakamoto, *Infrared and Raman Spectra of Inorganic and Coordination Compounds*, Wiley, New York, **1986**.
[16] N. Trendafilova, G. S. Nikolov, G. Bauer, R. Kellner, *Inorg. Chim. Acta* **1993**, *210*, 77.
[17] L. Chen, L. K. Thompson, J. N. Bridson, *Inorg. Chem.* **1993**, *32*, 2938.
[18] R. Minkwitz, M. Berkei, R. Ludwig, *Inorg. Chem.* **2001**, *40*, 25.
[19] W. J. Geary, *Coord. Chem. Rev.* **1971**, *7*, 21.
[20] G. B. Carpenter, *Acta Crystallogr.* **1966**, *20*, 334.
[21] A. Bencini, D. Gatteschi, *EPR of Exchange Coupled Systems*, Springer-Verlag, Berlin, **1990**.
[22] C. F. Martens, A. P. H. J. Schenning, M. C. Feiters, J. Heck, P. T. Beurskens, E. Steinwender, R. J. M. Nolte, *Inorg. Chem.* **1993**, *32*, 3029.
[23] R. J. M. Klein Gebbink, C. F. Martens, P. J. A. Kenis, R. J. Jansen, H.-F. Nolting, V. A. Solé, M. C. Feiters, K. D. Karlin, R. J. M. Nolte, *Inorg. Chem.* **1999**, *38*, 5755.
[24] M. Louloudi, K. Mitopoulou, E. Evaggelou, Y. Deligiannakis, N. Hadjiliadis, *J. Mol. Catal. A: Chem.* **2003**, *198*, 231.
[25] A. D. Becke, *J. Chem. Phys.* **1992**, *96*, 2155.
[26] A. D. Becke, *J. Chem. Phys.* **1993**, *98*, 5648.
[27] C. Lee, W. Yang, R. G. Parr, *Phys. Rev. B* **1988**, *37*, 785.
[28] W. R. Wadt, P. J. Hay, *J. Chem. Phys.* **1985**, *82*, 5284.
[29] J. B. Nicholas, *Top. Catal.* **1997**, *4*, 157.
[30] W. R. Koch, H. Hertwing, *Chem. Phys. Lett.* **1997**, *268*, 345.
[31] L. A. Curtis, K. Raghavachari, P. C. Redfern, J. A. Pople, *Chem. Phys. Lett.* **1997**, *270*, 419.
[32] D. M. Smith, B. T. Golding, L. Radom, *J. Am. Chem. Soc.* **1999**, *121*, 9388.
[33] A. K. Ghandra, M. T. Nguyen, *Chem. Phys.* **1998**, *232*, 299.
[34] J. B. Nicholas, *Top. Catal.* **1999**, *9*, 181.
[35] R. Arnaud, C. Adamo, M. Cossi, A. Millet, Y. Valle, V. Barone, *J. Am. Chem. Soc.* **2000**, *122*, 324.
[36] H. B. Schlegel, *J. Comput. Chem.* **1982**, *3*, 214.
[37] R. Bauernschmitt, R. Ahlrichs, *Chem. Phys. Lett.* **1996**, *256*, 454.
[38] C. Jamorski, M. E. Casida, D. R. Salahud, *J. Chem. Phys.* **1996**, *104*, 5134.
[39] S. J. A. van Gisbergen, F. Kootstra, P. R. T. Schipper, O. V. Gritsenko, J. G. Snijders, E. Baerends, *J. Phys. Rev. A* **1998**, *57*, 1556.
[40] A. Rosa, E. J. Baerends, S. J. A. van Gisbergen, E. van Lenthe, J. A. Groeneveld, J. G. Snijders, *J. Am. Chem. Soc.* **1999**, *121*, 10356.
[41] S. J. A. van Gisbergen, J. A. Groeneveld, A. Rosa, J. G. Snijders, E. J. Baerends, *J. Phys. Chem. A* **1999**, *103*, 6835.
[42] P. Boulet, H. Chermette, C. Daul, F. Gilardoni, F. Rogemond, J. Weber, G. Zuber, *J. Phys. Chem. A* **2001**, *105*, 885.
[43] M. J. Frisch, G. W. Trucks, H. B. Schlegel, G. E. Scusseria, M. A. Robb, J. R. Cheeseman, V. G. Zakrzewski, J. A. Montgomery, R. E. Stratmann, J. C. Burant, S. Dapprich, J. M. Mil-

lan, A. D. Daniels, K. N. Kudin, M. C. Strain, O. Farkas, J. Tomasi, V. Barone, M. Cossi, R. Cammi, B. Mennucci, C. Pomelli, C. Adamo, S. Clifford, J. Orchterski, G. A. Petersson, P. Y. Ayala, Q. Cui, K. Morokuma, D. K. Malick, A. D. Rabuck, K. Raghavachari, J. B. Foresman, J. Cioslowski, J. V. Ortiz, B. B. Stefanov, G. Liu, A. Liashenko, P. Piskorz, I. Komaroni, R. Gomperts, R. L. Martin, D. J. Fox, T. Keith, M. A. Al-Laham, C. Y. Peng, A. Nanayakkara, C. Gonzalez, M. Challacombe, P. M. Gill, P. Johnson, W. Chen, M. W. Wong, J. L. Andres, M. Head-Gordon, E. S. Replogle, J. A. Pople, *Gaussian03*, revision A.7, Gaussian Inc., Pittsburgh, PA, **1998**.

[44] Cambridge Scientific Computing Inc., 875 Massachusetts Ave., Suite 41, Cambridge, MA 02139.

[45] N. F. Curtis, H. K. J. Powell, *J. Chem. Soc. A* **1968**, 3069.

[46] Z. Otwinowski, W. Minor, in *Macromolecular Crystallography*, vol. 276 (Eds.: C. W. Carter, Jr., R. M. Sweet), Academic Press, New York, **1997**, p. 307.

[47] R. Hooft, N. B. V., Delft, The Netherlands, **1998**.

[48] A. Altomare, M. C. Burla, M. Camalli, G. L. Cascarano, C. Giacovazzo, A. G. G. Moliterni, G. Polidori, R. Spagna, *J. Appl. Crystallogr.* **1994**, *27*, 435.

[49] G. M. Sheldrick, University of Göttingen, Göttingen, Germany, **1997**.

[50] L. J. Farrugia, *J. Appl. Crystallogr.* **1997**, *30*, 565.

Received: February 18, 2005
Published Online: August 2, 2005

